A Computational Study on Some Viable Targets for Gas-Phase Synthesis of Metal Complexes of the Cyclic $(B_6C)^{-2}$ and Their Bonding Pattern

Shant Shahbazian* and Shadi Alizadeh

Department of Chemistry, Faculty of Sciences, P.O. Box 19395-4716, Shahid Beheshti University, Evin, Tehran, Iran 19839

Received: August 1, 2008; Revised Manuscript Received: August 13, 2008

In this account, a detailed computational study is conducted to verify the geometric, energetic, and electronic properties of the planar cyclic $(B_6C)^{-2}$ (as the simplest carrier of hexacoordinate carbon) within some metal complexes. The $[M(B_6C)]^{(-)}$ (M = *Li*, *Na*, *K*) and $[M(B_6C)]$ (M = *Be*, *Mg*, *Ca*) series are employed for this purpose. Relevant ab initio calculations at both DFT and post-HF levels vividly demonstrate that this dianion is stabilized considerably in the electric field generated by cations, whereas the geometrical and electronic properties of this ring remain almost intact in these complexes. The complementary topological analysis of charge densities confirms that cyclic $(B_6C)^{-2}$ within these complexes exhibits the same topological patterns as the naked dianion, thus confirming the presence of an unusual charge density distribution in this dianion. An electrostatic model is proposed that not only qualitatively but also quantitatively explains the observed computational trends in these complexes. This model successfully traces the polarization of the central carbon atom of the ring in the presence of a hard, multiply charged cation. To facilitate experimental detection, the photoelectron spectra of the $[M(B_6C)]^{(-)}$ (M = *Li*, *Na*, *K*) series are computed and the dominant features are extracted. Although considered species are not global minima on their potential energy hypersurfaces, their kinetic stabilities are verified and demonstrated unequivocally.

1. Introduction

Small planar or quasi-planar boron clusters have recently attracted a lot of attention.[1−7] Their unusual geometries and bonding modes make them attractive (and in the same way challenging) for both theoretical and experimental chemists. In this regard, boron wheels are probably the most intriguing members of this class of clusters. Accordingly, an atom or a group of atoms may be trapped in the middle of these molecular wheels. These trapped atoms are usually hypercoordinate species with no similar examples. On the other hand, serious deviations from the classic structural rules of organic chemistry were (and are) always an intriguing (and at the same time challenging) issue for organic chemists.[8,9] This area is the territory of bizarre entities (planar, hypercoordinate, unusually strained,... carbon-containing molecules) that may even challenge the imagination of the most experienced synthetic chemists. Since the seminal proposal of Hoffmann and co-workers,[10] computational studies on the planar and hypercoordinate-containing carbon molecules have been in central focus.[11−16] Subsequent experimental activities also confirmed possible realization of some of these species.[17,18]

The cyclic $(B_6C)^{-2}$ (Figure 1) may be conceived as one of these strange species that was first proposed by Schleyer and co-workers on the basis of their computational studies.[19,20] Since then, a wealth of computational studies have been conducted to elucidate different features of this species and similar hypercoordinate atoms within boron wheels.[21−40] In this accord, in two recent articles,[35,37] we considered the bonding pattern of this species and similar molecules employing the quantum theory of atoms in molecules (QTAIM)[41] in some detail. Although novel patterns emerged from our analysis, our subsequent ab initio calculations[36] (in line with others[31]) demonstrated that this dianion is unstable against electron autodetachment. Thus, a question that arises naturally is how it is possible to make this unstable dianion a stable entity and at the same time retain its novel bonding pattern. Indeed, some recent computational investigations unequivocally established that cyclic $(B_6C)^{-2}$ may be combined with various alkali, alkali earth, and transition metals and that it retains its geometrical and electronic identity.[30,31,34,39,40] In all of these studies, the main focus was on designation of novel and stable sandwich-type complexes involving metallocene-like as well as triple and tetra-decker species. Although these state-of-the-art complex designations are indeed interesting, there are yet unanswered questions that remain to be verified. These questions may be categorized into two main classes. The first class includes questions relevant to the details of bonding pattern in these species: "Is the novel bonding pattern of $(B_6C)^{-2}$ retained in corresponding com-

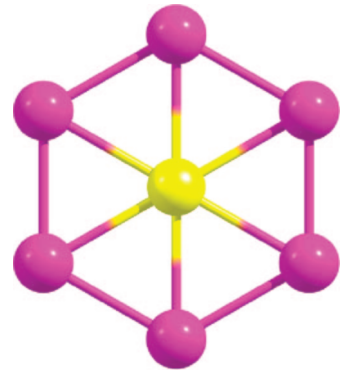

Figure 1. Molecular geometry of planar $(B_6C)^{-2}$ dianion. The pink spheres represent boron atoms, whereas the central yellow one represents the carbon atom.

* To whom correspondence should be addressed. Tel./Fax: 98-21-22431661. E-mail: chemist_shant@yahoo.com.

10.1021/jp806874u CCC: $40.75
Published on Web 09/25/2008

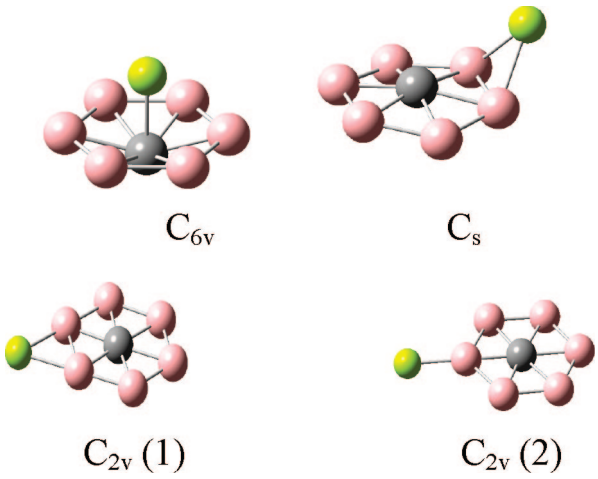

Figure 2. Optimized geometries of metal complexes in this study (the relevant point group symmetries are also offered in this figure). Yellow spheres are metal atoms, whereas gray spheres are carbon atoms.

TABLE 1: Relative Energies (RE) and the Number of Imaginary Frequencies (NIMAG) Calculated for Different Optimized Structures at the B3LYP/6-311+g(d) Level

		conformer[a]			
molecule		C_{6v}	C_s	$C_{2v}(1)$	$C_{2v}(2)$
$Be(B_6C)$	NIMAG	0	0	1	2
	RE[b]	0.0	21.6	57.3	80.1
$Mg(B_6C)$	NIMAG	2	0	2	2
	RE[b]	7.3	0.0	45.2	58.3
$Ca(B_6C)$	NIMAG	0		2	2
	RE[b]	0.0		52.4	59.9
$Li(B_6C)^{(-1)}$	NIMAG	0		2	2
	RE[b]	0.0		34.1	43.3
$Na(B_6C)^{(-1)c}$	NIMAG	0		0	2
	RE[b]	0.0		23.8	30.0
	NIMAG	0		2	3
	RE[b]	0.0		25.8	32.0
$K(B_6C)^{(-1)c}$	NIMAG	0		0	3
	RE[b]	0.0		26.1	29.3
	NIMAG	0		2	
	RE[b]	0.0		30.1	

[a] The general structures of each symmetry type are depicted in Figure 2 within the text. [b] Relative electronic energies (kcal mol^{-1}) without zero point corrections. [c] The second row contains the same information at the MP2/6-311+g(d) level.

plexes?" or "What are the effects of cations on the charge density distribution of this dianion?" Thus, in this study, the previous QTAIM analysis will be performed on some selected complexes. On the other hand, the second class of questions is directed toward successful (gas-phase) synthesis and detection of these species: "What are the most viable targets for gas-phase synthesis?" or "How may theoretical calculations assist detection of synthesized complexes?" These and similar questions are also the main concern of this article. Therefore, in this study, we will also focus on the thermodynamic and kinetic stability of the cyclic $(B_6C)^{-2}$.

Accordingly, we also employed many metal cations in our computational investigations, and from an extensive considered set only a subset, namely, $[M(B_6C)]^{(-)}$ (M = *Li*, *Na*, *K*) and $[M(B_6C)]$ (M = *Be*, *Mg*, *Ca*), will be scrutinized in this article. Cations are selected on the basis of a detailed search of recent literature that deals with experimentally identified (exclusively in gas phase) multiply charged anions that were stabilized with proper countercations.[42] On the other hand, we are also interested in viable targets that may be traced by sophisticated spectroscopic methods in molecular beams. The laser photoelectron spectroscopy of monoanions (within molecular beams), as developed by Wang and co-workers,[43−45] seems to be the best candidate on the basis of recent successful applications.[42] Thus, the photoelectron spectra of stable conformers of negatively charged species are also computed in this article. A detailed topological analysis of the charge densities of metal complexes is done to verify the bonding pattern in these species.

We hope that this contribution and relevant computations therein may shed some light on the very nature of bonding of metal−$(B_6C)^{-2}$ complexes and at the same time be helpful for experimental characterization of proper complexes.

2. Computational Details

The ab initio calculations on the complexes were performed employing the well-known MP2[46,47] and B3LYP[48−50] methods in conjunction with series of Pople-type basis sets, namely, 6-31g(d), 6-311+g(d), and 6-311+g(2df).[51−54] First, initial geometries were optimized (within frozen core approximation), and then the frequency calculations were done to check the nature of optimized geometries. Only singlet ground states were considered in this study. The photoelectron spectra were constructed employing both the outer valence green's function (OVGF)[55−57] and the time-dependent density functional theory (TD-DFT) methods.[58−60] The whole series of ab initio calculations were done utilizing the Gaussian 98 suite of programs.[61] Then, "wfn" protocols (text files containing state function of the system) were extracted from ab initio calculations and were employed for topological analysis of electronic charge densities. Technical details may be found elsewhere.[35,37] The whole topological analysis was done utilizing the AIM2000 package.[62−64] Subsequently, comprehensive ab initio calculations were done to verify the stability of the cyclic dianion in regard to isomerization. To survey the singlet, ground potential energy hypersurface of $(B_6C)^{-2}$, a large number of initial geometries were constructed and then employed for primary geometry optimization. Because the kinetic stability of cyclic $(B_6C)^{-2}$ was the main concern of this study, the construction scheme of initial geometries, which was based on a mixture of chemical intuition and the outcome of previous studies,[4,7] was inevitably biased toward this goal. Therefore, in this study no attempt was made to employ automatic geometry generator algorithms. All initial structures were first optimized at the B3LYP/6-311+g(d) level, and then the optimized geometries were used for a secondary geometry optimization at the B3LYP/6-311+g(2df) level. Since the qualitative aspects of optimized structures are usually (but not always) similar at these two computational levels, only the results at the B3LYP/6-311+g(2df)level are reported. In this article, we will concentrate only on local minima and transition states (first-order saddle points), and as a result higher order saddle points are all neglected. The Cartesian coordinates and total energies of all optimized structures are gathered in Supporting Information. To verify the nature of optimized geometries, harmonic frequencies were calculated for each optimized structure. Subsequently, all transition states were analyzed by the intrinsic reaction coordinate (IRC) method and proper local minima were located at both sides of reaction coordinates (at the B3LYP/6-311+g(d) level).[65,66] Subsequently, a single point calculation was done employing ab initio MP2,[46,47] MP3,[67,68] and MP4(SDQ)[69] as well as CCSD and CCSD(T) methods[70,71] in conjunction with the aug-cc-pVDZ basis set[72−74] on all optimized structures. Finally, some complementary calculations were done for better evaluation of the main kinetic barriers.

TABLE 2: Selected Geometrical Parameters and the Energetic Values of Metal−$(B_6C)^{-2}$ Complexes Considered in This Study and the Naked $(B_6C)^{-2}$ at the B3LYP/6-311+g(2df) and MP2/6-311+g(2df) Levels

		internuclear distances				dissociation energies		point charge model[b]	
molecule[a]	method	B−B	B−C	metal−C	metal−B	D_e	D_0	ΔE	percent
$Be(B_6C)$	B3LYP	1.571	1.631	1.701	2.017	709.7	706.9	913.6	78
	MP2	1.588	1.641	1.698	2.041	694.8	691.8	863.5	80
$Mg(B_6C)$	B3LYP[c]	1.586	1.603	2.080	2.431	555.4	554.1	857.5	65
	MP2	1.601	1.616	2.081	2.456	542.5	541.3	827.0	66
$Ca(B_6C)$	B3LYP	1.577	1.592	2.406	2.693	496.7	494.6	822.8	60
	MP2	1.593	1.606	2.368	2.685	488.1	486.0	796.1	61
$Li(B_6C)^{(-1)}$	B3LYP	1.580	1.594	1.969	2.362	250.9	248.5	278.6	90
	MP2	1.596	1.607	1.986	2.400	246.3	244.0	276.4	89
$Na(B_6C)^{(-1)}$	B3LYP	1.585	1.588	2.353	2.754	217.9	216.6	246.2	88
	MP2	1.600	1.603	2.380	2.794	213.1	211.8	243.4	88
$K(B_6C)^{(-1)}$	B3LYP	1.583	1.586	2.722	3.075	197.5	196.3	220.5	90
	MP2	1.599	1.601	2.678	3.049	200.7	199.3	222.6	90
$B_6C^{(-2)}$	B3LYP	1.587	1.587						
	MP2	1.602	1.602						

[a] Only the C_{6v} (see Figure 2) structure is considered in this table. [b] A point charge is deposited in place of each cation, and the calculated energies are compared with naked dianion. The percent column offers the percent ratio of ab initio and point charge related dissociation energies. [c] Geometrical parameters and dissociation energies are those of the C_{6v} structure that is a second-order saddle point (energy difference with stable C_s structure is only 6.3 kcal mol^{-1}). Structural information of the stable C_s structure may be found in Supporting Information.

TABLE 3: QTAIM Atomic Charges and the Results of Point Charge Calculations[a] of Metal−$(B_6C)^{-2}$ Complexes at the B3LYP/6-311+g(2df) Level

	QTAIM atomic charges					point charge model		
molecule	metal	C	B	sum	metal[b]	Q[c]	ΔE[c]	percent[c]
$Be(B_6C)$	1.53	−2.19	0.11	0.00	1.62	1.75	703.1	99
$Mg(B_6C)$	1.64	−2.16	0.09	0.04	1.71	1.55	543.8	98
$Ca(B_6C)$	1.43	−2.14	0.12	0.04	1.54	1.50	501.7	99
$Li(B_6C)^{(-1)}$	0.85	−2.16	0.05	−1.02		0.9	243.1	97
$Na(B_6C)^{(-1)}$	0.85	−2.18	0.05	−1.01		0.9	216.4	99
$K(B_6C)^{(-1)}$	0.82	−2.19	0.06	−1.01		0.9	194.9	99

[a] See text for details. [b] The results at the MP2/6-311+g(2df) level. [c] "Q" is the optimum point charge that reproduces the ab initio dissociation energy, whereas "percent" is the percent ratio of ab initio and point charge-derived dissociation energies (ΔE).

3. Results and Discussion

3.1. Geometries and General Structures. To check all possibilities, various initial geometries were constructed for geometry optimization and then B3LYP/6-31g(d) was employed to locate stationary points on the potential energy surface. Figure 2 depicts some of the low-energy-optimized structures and their spatial symmetries. These stationary points were utilized for further optimization at the B3LYP/6-311+g(d) and MP2/6-311+g(d) levels. Table 1 offers the energy ordering and the nature of these stationary points. It is evident from this table that only C_{6v} or C_s structures are unambiguous true local minima. Indeed, from six molecules considered in this study, in four cases (M = *Li*, *Na*, *K*, *Ca*) C_{6v} structure is the only stable structure. This is in line with the most recent studies.[31,34] Even though in the case of (M = *Be*) at the MP2/6-311+g(d) level the only stable point in the considered region of its potential energy surface is the C_{6v} structure, two stable structures (C_{6v} and C_s) were found at the B3LYP/6-311+g(d) level. In the case of (M = *Mg*), the C_s structure is the only stable structure at both computational levels. To further scrutinize the nature of optimized structures, a full geometry optimization was done at the B3LYP/6-311+g(2df) and MP2/6-311+g(2df) levels. Supporting Information contains all relevant information, whereas Table 2 summarizes the main features and parameters.

At these computational levels, the C_{6v} structure remains the only local minima for (M = *Li*, *Na*, *K*, *Ca*). In the case of (M = *Be*), from the two competing structures (C_{6v} and C_s) at the B3LYP/6-311+g(2df) level, the C_{6v} structure is ∼21 kcal mol^{-1} more stable than C_s. To gain some insight into the kinetic stability of the C_s structure, the relevant transition state was located at this level. The barrier height of ($C_s \rightarrow C_{6v}$) transformation is only 1.1 kcal mol^{-1}. This vividly demonstrates that the C_s structure is not only thermodynamically but also kinetically unstable. Complementary calculations at the MP2/6-311+g(2df) level also confirm this picture. Therefore, it is safe to claim that the C_{6v} structure is the only stable structure of the $Be(B_6C)$ complex. In the case of (M = *Mg*), the C_s structure remains the only stable structure at the B3LYP/6-311+g(2df) level, whereas, inversely, the C_{6v} structure is the only stable entity at the MP2/6-311+g(2df) level. This discrepancy casts some doubt regarding the true nature of optimized geometries. In this study, we will assume that the results gained at the MP2/6-311+g(2df) level are more reliable than those derived at the B3LYP/6-311+g(2df) level since there is no a priori reason to believe that the interaction of *Mg* with cyclic dianion must be different from *Be* and *Ca*. Thus, although we will employ C_{6v} structure for subsequent discussions, probably a couple cluster method (CCSD or CCSD(T)) in conjunction with an extended basis set may unambiguously confirm this assumption.[75] It is worthwhile to stress that to the best of our knowledge, this is the first time that C_{6v} structures of $Be(B_6C)$ and $Mg(B_6C)$ complexes are reported in literature. In a recent article, Luo et. al stated, "However, attempts to optimize the geometries of C_{6v} [(η^6-B_6C)Be] and C_{6v} [(η^6-B_6C)Mg] are frustrated".[34] Our results are not in line with this conclusion, and it seems that their observation is probably rooted in their employed computational level or chosen initial geometries.

A quantitative comparison with the geometry of the naked dianion may be helpful to gain some insight into the bonding mechanism. In this regard, inspection of the geometrical parameters in Table 2 demonstrates that the ring preserves its geometrical integrity within these complexes. There are slight geometrical perturbations in these complexes that seem to have an inverse correlation with the metal atom's distance from carbon and boron atoms of the ring. Accordingly, the most perturbed ring is $Be(B_6C)$ since in this series of complexes, beryllium atom is located nearest the atoms of the ring. Even in this case, general structural features are completely similar

TABLE 4: Vertical Detachment Energies of C_{6v} Structures of $M(B_6C)^{-1}$ (M = *Li*, *Na*, *K*) Complexes Calculated at the OVGF/6-311+g(2df) and TD-B3LYP/6-311+g(2df) Levels

	B3LYP-optimized geometry					MP2-optimized geometry			
molecule	MO[a]	Koopman	OVGF	PS[b]	TD-B3LYP[c]	Koopman	OVGF	PS[b]	TD-B3LYP[c]
$Li(B_6C)^{-1}$	$4e_1$	2.23	2.53	0.89	2.47	2.19	2.50	0.89	2.44
	$3e_1$	5.37	4.70	0.89	4.61	5.32	4.65	0.88	4.56
	$1b_1$	6.37	5.10	0.88	5.03	6.32	5.06	0.88	5.02
	$6a_1$	8.28				8.29			
	$2e_2$	9.13	7.49	0.87		9.11			
	$5a_1$	9.67				9.51			
$Na(B_6C)^{-1}$	$5e_1$	1.72	2.00	0.89	1.95	1.69	1.97	0.89	1.92
	$4e_1$	5.01	4.29	0.88	4.15	4.99	4.26	0.88	4.22
	$1b_1$	6.03	4.81	0.76	4.63	5.98	4.69	0.84	4.68
	$8a_1$	8.00				8.02	6.77	0.62	
	$2e_2$	8.80				8.78			
	$7a_1$	9.13				8.97			
$K(B_6C)^{-1}$	$6e_1$	1.39	1.69	0.89	1.63	1.41	1.71	0.89	1.65
	$5e_1$	4.73	4.05	0.88	3.97	4.73	4.05	0.88	3.99
	$1b_1$	5.72	4.44	0.88	4.43	5.70	4.44	0.88	4.41
	$10a_1$	7.71				7.76			
	$2e_2$	8.49				8.47			
	$9a_1$	8.60				8.50			

[a] The involved canonical molecular orbital in excitation process. [b] The excitations that their pole strength (PS) is smaller than 0.6 in OVGF calculations are not reported in this table. [c] Only the first three excitations were calculated.

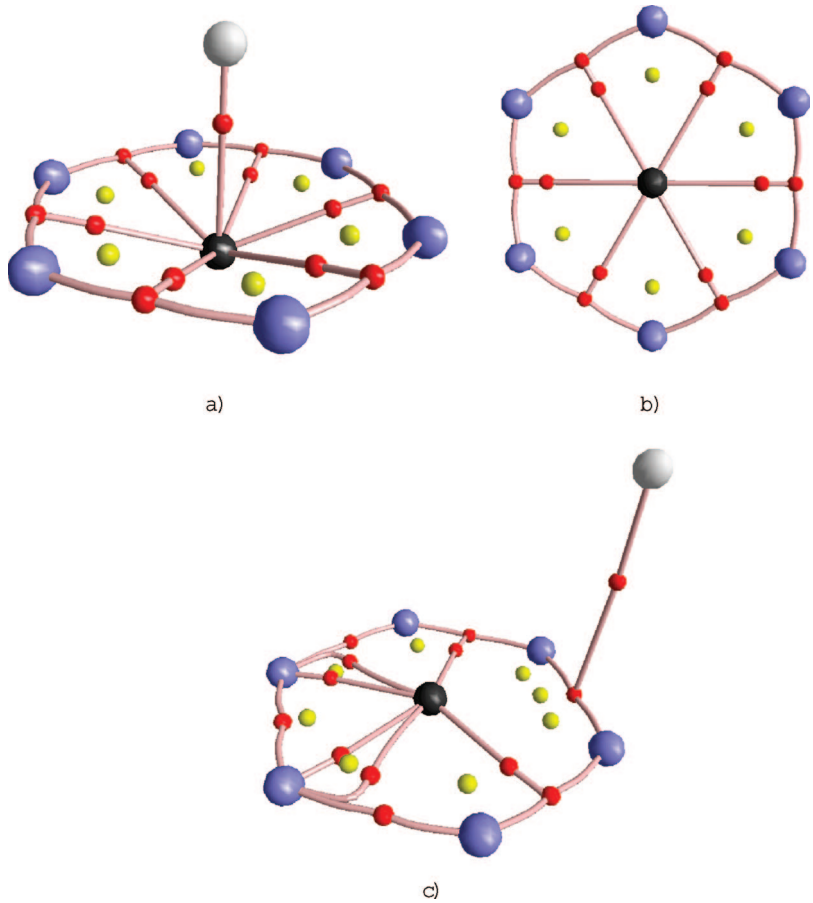

Figure 3. Observed general molecular graph of the metal complexes (a) and the naked dianion (b). The black and white spheres are carbon and metal atoms, respectively, whereas the six blue spheres are boron atoms. Red spheres are BCPs, whereas yellow spheres are RCPs. The shape (c) depicts the molecular graph of the C_s structure of the $Mg(B_6C)$ complex computed at the B3LYP/6-311+g(2df) level.

to the naked dianion. Other geometrical features and related patterns are similar to those described in previous studies, and we will not reiterate them here.[31,34,39]

3.2. Dissociation Energies. Table 2 offers dissociation energies (or inversely the association energies) of all considered complexes at the B3LYP/6-311+g(2df) and MP2/6-311+g(2df) levels. Both computational levels are quantitatively in accordance with each other and a previous study.[34] In contrast to our exceptions, dissociation energies are distributed within a large range namely from ~700 (M = *Be*) to ~200 (M = *K*) kcal mol^{-1}. This wide distribution needs some verification and a proper explanation.

TABLE 5: Topological Characters of B_6C Moiety at Equilibrium Geometries of All Considered Species Calculated at the MP2/6-311+g(2df) Level[a]

molecule	type of CP	ρ_c	$\nabla^2\rho_c$	λ_1	λ_2	G_b	H_b	G_b/ρ_c	H_b/ρ_c
$Be(B_6C)$									
	BCP(B,B)	0.16	−0.29	−0.18	−0.14	0.06	−0.13	0.37	−0.84
	BCP(C,BCP)	0.14	0.00	−0.14	−0.01	0.09	−0.09	0.61	−0.62
	RCP(B,C)	0.13	0.27	−0.13	0.04	0.19	−0.12	1.42	−0.91
$Mg(B_6C)$									
	BCP(B,B)	0.15	−0.26	−0.17	−0.11	0.06	−0.12	0.39	−0.82
	BCP(C,BCP)	0.14	−0.04	−0.15	0.00	0.08	−0.09	0.58	−0.65
	RCP(B,C)	0.14	0.33	−0.15	0.02	0.21	−0.12	1.51	−0.91
$Ca(B_6C)$									
	BCP(B,B)	0.15	−0.26	−0.17	−0.11	0.06	−0.13	0.40	−0.82
	BCP(C,BCP)	0.14	−0.05	−0.16	−0.01	0.08	−0.10	0.58	−0.66
	RCP(B,C)	0.14	0.34	−0.15	0.02	0.21	−0.13	1.52	−0.91
$Li(B_6C)^{(-1)}$									
	BCP(B,B)	0.15	−0.26	−0.17	−0.11	0.06	−0.13	0.40	−0.82
	BCP(C,BCP)	0.14	−0.05	−0.16	0.00	0.08	−0.10	0.57	−0.66
	RCP(B,C)	0.14	0.34	−0.16	0.02	0.21	−0.13	1.52	−0.91
$Na(B_6C)^{(-1)}$									
	BCP(B,B)	0.15	−0.25	−0.17	−0.10	0.06	−0.12	0.40	−0.82
	BCP(C,BCP)	0.14	−0.06	−0.16	0.00	0.08	−0.10	0.56	−0.66
	RCP(B,C)	0.14	0.35	−0.16	0.01	0.21	−0.13	1.54	−0.91
$K(B_6C)^{(-1)}$									
	BCP(B,B)	0.15	−0.25	−0.17	−0.10	0.06	−0.12	0.41	−0.82
	BCP(C,BCP)	0.14	−0.06	−0.16	0.00	0.08	−0.10	0.56	−0.67
	RCP(B,C)	0.14	0.35	−0.16	0.01	0.21	−0.13	1.54	−0.91
$B_6C^{(-2)}$									
	BCP(B,B)	0.15	−0.24	−0.17	−0.10	0.06	−0.12	0.40	−0.81
	BCP(C,BCP)	0.14	−0.06	−0.16	0.00	0.08	−0.10	0.55	−0.66
	RCP(B,C)	0.14	0.35	−0.16	0.01	0.21	−0.13	1.53	−0.91

[a] All values are in atomic units. For a comprehensive description of each index, see the relevant references.[35,37,41]

TABLE 6: Topological Characters of the BCPs between Metal and B_6C Moiety at Equilibrium Geometries of All Considered Species Calculated at the B3LYP/6-311+g(2df) and MP2/6-311+g(2df) Levels[a]

method	type of CP	ρ_c	$\nabla^2\rho_c$	λ_1	λ_2	G_b	H_b	G_b/ρ_c	H_b/ρ_c
B3LYP									
$Be(B_6C)$	BCP(Be,C)	0.07	0.44	−0.02	−0.02	0.13	−0.02	1.83	−0.27
$Mg(B_6C)^b$	BCP(Mg,C)	0.04	0.26	−0.02	−0.02	0.06	0.00	1.51	0.03
$Ca(B_6C)$	BCP(Ca,C)	0.04	0.20	0.00	0.00	0.05	0.00	1.31	0.06
$Li(B_6C)^{(-1)}$	BCP(Li,C)	0.03	0.21	−0.02	−0.02	0.05	0.00	1.55	0.15
$Na(B_6C)^{(-1)}$	BCP(Na,C)	0.02	0.13	−0.01	−0.01	0.03	0.00	1.31	0.19
$K(B_6C)^{(-1)}$	BCP(K,C)	0.04	0.20	0.00	0.00	0.05	0.00	1.31	0.06
MP2									
$Be(B_6C)$	BCP(Be,C)	0.07	0.47	−0.03	−0.03	0.14	−0.02	1.91	−0.26
$Mg(B_6C)$	BCP(Mg,C)	0.04	0.27	−0.02	−0.02	0.07	−0.02	1.91	−0.26
$Ca(B_6C)$	BCP(Ca,C)	0.04	0.21	−0.01	−0.01	0.05	0.00	1.59	0.05
$Li(B_6C)^{(-1)}$	BCP(Li,C)	0.03	0.21	−0.02	−0.02	0.05	0.00	1.30	0.01
$Na(B_6C)^{(-1)}$	BCP(Na,C)	0.02	0.13	−0.01	−0.01	0.03	0.00	1.60	0.16
$K(B_6C)^{(-1)}$	BCP(K,C)	0.02	0.10	−0.01	−0.01	0.02	0.00	1.38	0.22

[a] All values are in atomic units. For a comprehensive description of each index, see relevant references.[35,37,41] [b] This structure is a second-order saddle point.

In the case of the (M = *Li*, *Na*, *K*) series, dissociation energy smoothly diminishes from (M = *Li*) to (M = *K*). Intuitively, this pattern could be attributed to the distance of the cation from the ring and also to the very nature of electrostatic interactions. To test this hypothesis, metal atoms in the optimized geometries were replaced with a reference positive *point charge* ($Q = +1e$) and relevant dissociation energies were calculated for these artificial systems. The last two columns of Table 2 contain the final results at the B3LYP/6-311+g(2df) and MP2/6-311+g(2df) levels. They vividly demonstrate that the dissociation energies of this series of molecules, irrespective of the computational level, is always ~90% of the associated artificial counterparts. To verify the nature of interactions, the charge content of reference point charge was varied in ($\Delta Q = 0.1$ e) steps and associated dissociation energies were calculated at the B3LYP/6-311+g(2df) level. Tables 3 and S1 in the Supporting Information contain the final results. It is evident from these tables that a proper point charge ($Q = +0.9$ e) may reproduce the calculated dissociation energies with a high precision. The errors are less than 3% of total dissociation energies. Thus, it seems that the interaction of cations in this series with the anion may be simulated with electrostatic interaction of an effective point charge and the cyclic dianion. Independent calculation of atomic charges within QTAIM's methodology[41] also confirms this picture. Table 3 offers the atomic charges of metal atoms. In the (M = *Li*, *Na*, *K*) series, the atomic charges are almost constant and somewhere between +0.8 e and +0.9 e. These results are qualitatively and even quantitatively in line with point charge calculations. Accordingly, on the basis of these observations, one may claim that electrostatic forces are the dominant features of metal−ring interactions. Although this model does not dismiss a possible minor contribution of other types of interactions, it certainly confirms that there is no urgent need to invoke orbital-based models to explain the salient features of metal−ring interactions in this series (to avoid any confusion, we want to stress that our "electrostatic interactions" must be distinguished from the usual "electrostatic contributions" that are defined within various energy component analyses).[76−80]

TABLE 7: Intra-Atomic Electric Dipole Moments of Metal and Carbon Atoms of All Considered Species Calculated at the B3LYP/6-311+g(2df) Level[a]

	metal		carbon	
molecule	*d*(total)	$d(z)^b$	*d*(total)	$d(z)^b$
$Be(B_6C)$	0.15	0.15	1.38	1.38
$Mg(B_6C)$	0.12	0.12	0.57	0.57
$Ca(B_6C)$	0.10	0.10	0.30	0.30
$Li(B_6C)^{(-1)}$	0.04	0.04	0.30	0.30
$Na(B_6C)^{(-1)}$	0.05	0.05	0.19	0.19
$K(B_6C)^{(-1)}$	0.17	0.17	0.14	0.14

[a] All values are in debyes. [b] The *z*-axis is perpendicular to the $(B_6C)^{-2}$ plane and goes through metal and carbon atoms.

In the case of the (M = *Be*, *Mg*, *Ca*) series, the relevant dissociation energies also diminish from (M = *Be*) to (M = *Ca*). The results are independent from the employed computational level. To check the efficiency of point charge model in this series, a reference point charge ($Q = +2e$) was employed instead of metal cations. The relevant results are offered in the last columns of Table 2. In contrast to alkali metal complexes, there are significant differences between considered complexes. The percent ratio of dissociation energies of this model to the ab initio dissociation energies was lower than those of alkali metal complexes and diminishes from (M = *Be*) to (M = *Ca*). To verify the nature of metal−ring interactions, the charge content of reference point charge was varied in ($\Delta Q = 0.05$ e) steps and relevant dissociation energies were calculated at the B3LYP/6-311+g(2df) level. Tables 3 and S1 in the Supporting Information contain the final results. It is evident from these tables that the optimum point charge that may precisely reproduce the ab initio dissociation energies is different in these complexes; $Q = +1.75$ e for (M = *Be*), $Q = +1.55$ e for (M = *Mg*), and $Q = +1.50$ e for (M = *Ca*). Apparently, effective charges diminish from (M = *Be*) to (M = *Ca*). Independent calculation of atomic charges within QTAIM's methodology[41] does not seem to conform to this picture since the calculated atomic charges are $Q = +1.53$ e for (M = *Be*), $Q = +1.64$ e for (M = *Mg*), and $Q = +1.43$ e for (M = *Ca*). Whereas the

TABLE 8: Relative Energies (kcal mol^{-1}) of Different Species Calculated at the B3LYP/6-311+g(2df) and CCSD(T)/aug-cc-pVDZ Levels in Regard to Cyclic $B_6C^{(-2)}$[a]

number	B3LYP	CCSD(T)	NIMAG[b]	type of TS	number	B3LYP	CCSD(T)	NIMAG[b]	type of TS
1	0.0	0.0	0		**52**	**–0.7**	**–4.6**	1	2–53
2	**–21.0**	**–22.2**	0		**53**	**–13.2**	**–11.5**	0	
3	**–19.6**	**–19.9**	1	2–2	**54**	19.4	19.6	1	33–59
4	4.1	3.5	1	49–49(?)	**55**	15.9	12.4	1	2–60
5	**–8.8**	**–7.3**	0		**56**	**–6.6**	**–5.1**	1	20–37(?)
6	36.1	79.2	1	5–5	**57**	6.3	3.7	0	
7	22.5	12.2	0		**58**	10.2	6.0	1	2–57
8	39.6	36.6	0		**59**	16.9	19.3	0	
9	**–39.3**	**–37.6**	0		**60**	12.6	11.6	0	
10	30.7	26.2	0		**61**	23.6	20.8	1	33–9
11	33.2	30.6	1	14–15	**62**	17.1	18.5	1	57–59
12	40.8	36.3	1	1–17	**63**	**–5.5**	0.7	1	34–53
13	35.3	29.8	1	10–16	**64**	18.0	15.1	1	36–2
14	31.1	26.6	0		**65**	**–13.2**	**–12.0**	1	53–66
15	**–18.6**	**–17.2**	0		**66**	**–23.7**	**–23.4**	0	
16	27.8	24.7	0		**67**	**–18.4**	**–16.8**	1	15–66
17	30.6	22.5	0		**68**	9.3	11.4	1	42–49(?)
18	26.9	22.5	1	2–22	**69**	**–30.2**	**–27.4**	1	20–20(?)
19	29.8	11.9	0		**70**	**–5.4**	**–5.6**	1	20–9
20	**–40.6**	**–38.7**	0		**71**	**–6.4**	**–7.0**	1	20–9
21	19.9	5.3	0		**72**	**–5.1**	**–4.3**	0	
22	20.6	15.5	0		**73**	28.6	28.6	1	9–9(?)
23	40.9	33.6	1	15–17	**74**	22.6	24.6	1	37–37
24	38.8	33.7	1	1–14	**75**	20.9	16.8	0	
25	8.8	6.0	0		**76**	25.6	17.7	1	27–75
26	22.7	13.1	0		**77**	19.9	9.7	0	
27	17.8	8.4	0		**78**	34.3	24.4	0	
28	14.6	5.9	0		**79**	28.3	17.6	0	
29	20.7	20.3	0		**80**	19.6	10.4	0	
30	21.9	13.9	0		**81**	10.1	3.9	0	
31	13.3	9.6	0		**82**	26.0	16.3	0	
32	9.3	**–0.6**	0		**83**	23.1	15.6	0	
33	18.3	21.2	0		**84**	65.6	65.4	0	
34	**–7.9**	**–2.7**	0		**85**	26.4	27.6	0	
35	13.9	13.6	0		**86**	45.5	47.0	0	
36	14.5	13.1	0		**87**	30.7	30.1	0	
37	**–6.6**	**–5.0**	0		**88**	50.8	82.9	0	
38	2.7	5.1	0		**89**	39.4	44.8	0	
39	26.4	15.5	1	30–32	**90**	1.7	7.4	0	
40	28.1	18.2	0		**91**	18.5	24.1	0	
41	11.4	2.4	0		**92**	33.0	125.5	0	
42	9.2	10.9	0		**93**	29.4	35.0	0	
43	26.9	27.9	0		**94**	30.4	30.6	0	
44	30.9	21.5	1	17–32	**95**	28.8	32.1	0	
45	23.7	15.2	1	2–32	**96**	**–25.7**	**–20.8**	0	
46	47.4	43.9	1	1–43	**97**	13.9	17.0	0	
47	27.3	28.2	1	42–43	**98**	3.5	20.1	0	
48	9.7	7.8	1	15–49	**99**	0.7	–0.8	1	34–34
49	**–10.1**	**–10.6**	0		**100**	**–7.3**	**–1.3**	1	34–96
50	**–8.7**	**–7.4**	1	5–49	**101**	**–2.1**	**–1.1**	1	53–72
51	7.5	7.4	1	38–57					

[a] The B3LYP energies were corrected for zero point vibrations, whereas the CCSD(T) energies were derived from single point calculations at B3LYP-optimized geometries without ZPE corrections. The question marks in the last column were employed to emphasize that IRC was unable to fully locate both reactants and products in some cases. In such cases, additional geometry optimizations were done to locate the proper local minimum on both sides of reaction path. [b] Number of imaginary frequencies.

point charge electrostatic picture works well for (M = *Ca*), it deteriorates for (M = *Mg*) and (M = *Be*); the difference between these two types of charges increases considerably. As a final test, QTAIM charges were also computed at the MP2/6-311+g(2df) level. Although there is almost a constant increase (~0.1 e) in the metal charges, the main trends are similar to that observed at the B3LYP/6-311+g(2df) level. According to the point charge model, the effective charge of beryllium atom is more than that of magnesium atom in corresponding complexes, whereas the reverse is true for atomic charges that were calculated independently within the framework of QTAIM. Therefore, it seems that the simple point charge model fails to capture a proper physical picture governing metal−ring interactions for these two complexes. Although there is no doubt that electrostatic forces have a pivotal role in describing metal−ring interactions, they must be somehow modified to incorporate the apparent deviations from a simple point charge model. In this regard, many probable hypotheses may be proposed to explain the failure of this model and possible roots for proper modifications. On the other hand, one must also propose a mechanism that explains the constancy of atomic charges of metal atoms in alkaline−$(B_6C)^{-2}$ complexes as well as varied atomic charges

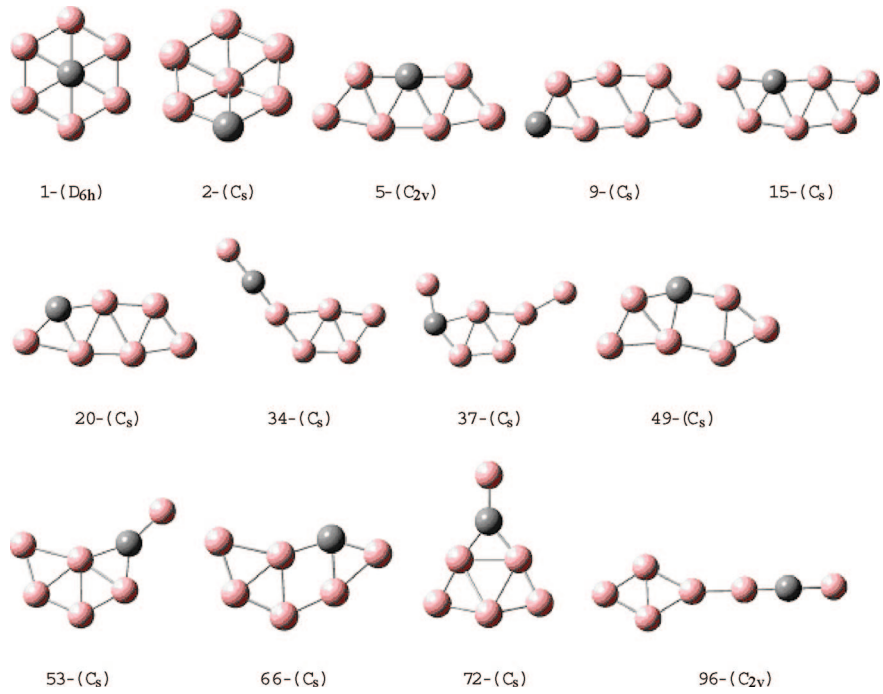

Figure 4. Structures of cyclic $(B_6C)^{-2}$ and the other more stable isomers. Gray spheres are carbon atoms, whereas pink spheres are boron atoms.

of metals in alkaline earth-based complexes. We postpone further discussion on these issues until after a detailed topological analysis of the charge densities of these complexes.

3.3. Photoelectron Spectra (PES). To facilitate the spectroscopic characterization of these complexes, PES of monoanions was calculated. The previous combined experimental and theoretical experiences[42] confirm that this is a powerful method for unambiguous characterization of geometry and electronic structure of bizarre species.

Table 4 offers the final results. To check the role of geometry variations on the calculated spectra, the optimized geometries at both the B3LYP/6-311+g(2df) and MP2/6-311+g(2df) levels were employed. The pole strengths were calculated for each detachment channel to verify the reliability of the OVGF method. On the other hand, to check the consistency of employed methods, both OVGF and TD-B3LYP methods were utilized to construct the spectra. The vertical detachment energies in Table 4 demonstrate that the calculated spectra have minor dependence on the geometrical variations and the method of calculation. In the range of ~1 to ~6 eV (that is the usual experimental window), three single-photon detachment channels were observed. All involved molecular orbitals are distinguished in Table 4. The main features are common among the three considered complexes. Relevant calculations predict three peaks around ~2.5, ~4.6, and ~5.0 eV for $Li(B_6C)^{-1}$, three peaks around ~2.0, ~4.2, and ~4.7 eV for $Na(B_6C)^{-1}$, and finally three peaks around ~1.7, ~4.0, and ~4.4 eV for $K(B_6C)^{-1}$. It is apparent that the detachment energies of all channels tend to diminish going from (M = *Li*) to (M = *K*). This is in line with the trend that was observed for dissociation energies; stronger electrostatic interactions stabilize cyclic dianion more efficiently, and this conforms to the observed large dissociation and electron detachment energies.

Although Koopman's theorem does not yield precise quantitative results for the low energy detachment energies (compare the numerical values in Table 4), on the basis of the computed orbital energies, there is less doubt that the higher energy detachment channels cannot be efficiently activated by 6 eV or lower energy photons. Therefore, the three aforementioned peaks must be the only dominant features in experimental spectra of corresponding complexes.

3.4. Topological Analysis of Charge Density Distribution. The topological analysis of charge densities is an efficient tool to characterize the very nature of bonding. Some recent excellent contributions[81−83] unequivocally established its ability within bonding realm. In two recent contributions, we also employed this method to consider the charge density distribution of the naked dianion.[35,37] These considerations result in interesting conclusions. Our results may be compressed as follows:

1. Detailed analysis of charge density distribution clearly demonstrates that the charge density between the central carbon atom and peripheral boron atoms is extremely flat and even a slight perturbation, such as zero point nuclear vibrations, may change the topological pattern and corresponding molecular graph. In other words, we are faced with an "isodensity" ring around the central carbon basin.
2. Evaluation of relevant topological indexes at bond critical points clearly demonstrates that the bonding mode of neighboring boron atoms within the rim of this ring is the usual "directional shared interactions", whereas central carbon and boron atoms of the rim participate in an unusual, probably novel "nondirectional shared interactions".
3. In contrast to the simple electronegativity arguments, the central carbon atom bears almost all of the extra negative charge of the ring (~−2.0 e).
4. All these observations are independent of the employed computational level and retain at various DFT and post-HF levels.

To check the role of metal atoms on charge density distribution and relevant topological indexes, the whole analysis was redone at both the B3LYP/6-311+g(2df) and MP2/6-311+g(2df) levels for all considered complexes and also the naked dianion. Final results are compressed in Figure 3 and Tables 5, 6, and S2 in the Supporting Information. First, we will concentrate on the ring.

TABLE 9: Relative Energies (kcal mol^{-1}) of All Intermediates that Are Involved in Various Destruction Channels of Cyclic $B_6C^{(-2)}$ to the More Stable Isomers

transformations	mechanisms														
1−2	1	TS	17	TS	32	TS	2								
B3LYP/6-311+g(2df)	0	40.8	30.6	30.9	9.3	23.7	−21.0								
CCSD(T)/aug-cc-pVDZ[a]	0	36.3	22.5	21.5	−0.6	15.2	−22.2								
1−15	1	TS	14	TS	15										
B3LYP/6-311+g(2df)	0	38.8	31.1	33.2	−18.6										
CCSD(T)/aug-cc-pVDZ[a]	0	33.7	26.6	30.6	−17.2										
1−5	1	TS	17	TS	15	TS	49	TS	5						
B3LYP/6-311+g(2df)	0	40.8	30.6	40.9	−18.6	9.7	−10.1	−8.7	−8.8						
CCSD(T)/aug-cc-pVDZ*	0	36.3	22.5	33.6	−17.2	7.8	−10.6	−7.4	−7.3						
1−9	1	TS	17	TS	32	TS	2	TS	57	TS	59	TS	33	TS	9
B3LYP/6-311+g(2df)	0	40.8	30.6	30.9	9.3	23.7	−21.0	10.2	6.3	17.1	16.9	19.4	18.3	23.6	−39.3
CCSD(T)/aug-cc-pVDZ*	0	36.3	22.5	21.5	−0.6	15.2	−22.2	6.0	3.7	18.5	19.3	19.6	21.2	20.8	−37.6
1−53	1	TS	17	TS	32	TS	2	TS	53						
B3LYP/6-311+g(2df)	0	40.8	30.6	30.9	9.3	23.7	−21.0	−0.7	−13.2						
CCSD(T)/aug-cc-pVDZ*	0	36.3	22.5	21.5	−0.6	15.2	−22.2	−4.6	−11.5						
1−49	1	TS	17	TS	15	TS	49								
B3LYP/6-311+g(2df)	0	40.8	30.6	40.9	−18.6	9.7	−10.1								
CCSD(T)/aug-cc-pVDZ*	0	36.3	22.5	33.6	−17.2	7.8	−10.6								
1−34	1	TS	17	TS	32	TS	2	TS	53	TS	34				
B3LYP/6-311+g(2df)	0	40.8	30.6	30.9	9.3	23.7	−21.0	−0.7	−13.2	−5.5	−7.9				
CCSD(T)/aug-cc-pVDZ*	0	36.3	22.5	21.5	−0.6	15.2	−22.2	−4.6	−11.5	0.7	−2.7				
1−20	1	TS	17	TS	32	TS	2	TS	57	TS	59	TS	33	TS	9
B3LYP/6-311+g(2df)	0	40.8	30.6	30.9	9.3	23.7	−21.0	10.2	6.3	17.1	16.9	19.4	18.3	23.6	−39.3
CCSD(T)/aug-cc-pVDZ*	0	36.3	22.5	21.5	−0.6	15.2	−22.2	6.0	3.7	18.5	19.3	19.6	21.2	20.8	−37.6
	TS	20													
	−5.4	−40.6													
	−5.6	−38.7													
1−37	1	TS	17	TS	32	TS	2	TS	57	TS	59	TS	33	TS	9
B3LYP/6-311+g(2df)	0	40.8	30.6	30.9	9.3	23.7	−21.0	10.2	6.3	17.1	16.9	19.4	18.3	23.6	−39.3
CCSD(T)/aug-cc-pVDZ*	0	36.3	22.5	21.5	−0.6	15.2	−22.2	6.0	3.7	18.5	19.3	19.6	21.2	20.8	−37.6
	TS	20	TS	37											
	−6.4	−40.6	−6.6	−6.6											
	−7.0	−38.7	−5.1	−5.0											
1−66	1	TS	17	TS	15	TS	66								
B3LYP/6-311+g(2df)	0	40.8	30.6	40.9	−18.6	−18.4	−23.7								
CCSD(T)/aug-cc-pVDZ*	0	36.3	22.5	33.6	−17.2	−16.8	−23.4								
1−96	1	TS	17	TS	32	TS	2	TS	53	TS	34	TS	96		
B3LYP/6-311+g(2df)	0	40.8	30.6	30.9	9.3	23.7	−21.0	−0.7	−13.2	−5.5	−7.9	−7.3	−25.7		
CCSD(T)/aug-cc-pVDZ*	0	36.3	22.5	21.5	−0.6	15.2	−22.2	−4.6	−11.5	0.7	−2.7	−1.3	−20.8		
1−~~53~~	1	TS	17	TS	32	TS	2	TS	53	TS	72				
B3LYP/6-311+g(2df)	0	40.8	30.6	30.9	9.3	23.7	−21.0	−0.7	−13.2	−2.1	−5.1				
CCSD(T)/aug-cc-pVDZ*	0	36.3	22.5	21.5	−0.6	15.2	−22.2	−4.6	−11.5	−1.1	−4.3				

[a] Single point calculation at B3LYP/6-311+g(2df)-optimized geometry without ZPE corrections.

Figure 3a,b depicts a typical molecular graph for these complexes and also for the naked dianion. These molecular graphs are insensitive to the employed computational level and also to the type of metal atom. Both molecular graphs are "conflict catastrophes" (for technical details and relevant nomenclature, see our previous contributions),[35,37,41] and so they are topologically unstable entities. This means that even a slight perturbation of nuclear geometries must vary this molecular graph. Figure 3c depicts this fact vividly. This molecular graph corresponds to the C_s structure of the $Mg(B_6C)$ complex at the B3LYP/6-311+g(2df) level. The energy content of this structure differs from the C_{6v} structure by only 6.3 kcal mol^{-1}. However, a new molecular graph emerges at this geometry. The flatness of charge density distributions of these complexes is evident from these observations. Tables 5 and 6 confirm this fact quantitatively. In all considered complexes and also the naked dianion, the difference between the amount of charge density at bond and ring critical points, which are located around the central carbon atom, namely, BCP(C,BCP) and RCP(B,C), is negligible. On the other hand, λ_2, the negative curvature of charge density along an axis in the plane of the ring that is perpendicular to bond path at BCP and corresponding positive curvature at RCP, is also close to zero. Both these facts clearly confirm that we are faced with "topologically floppy" molecules.[35,37] Tables 5 and S2 in the Supporting Information also contain topological indexes at bond and ring critical points. Inspection of these tables clearly reveals that there is no serious difference between the bonding mode of the naked and bonded dianions. Like molecular geometries, the most pronounced perturbations are those of the $Be(B_6C)$ complex, although even in this case the general patterns are not affected. Therefore, in line with previous studies,[35,37] the bonding mode of neighboring boron atoms is directional shared interactions, whereas that of central carbon and peripheral boron atoms is a nondirectional shared interaction (for technical details, see original references). All these facts demonstrate that the topological characteristics and the bonding modes of considered rings (within complexes) are virtually indistinguishable from the naked dianion. Apparently, metal atoms have no serious effect on the topological structure of charge density and associated topological characteristics. Table 3 contains the atomic charges of carbon and boron atoms. Once again, we found no serious difference with the naked dianion. Carbon's basin contains all the extra negative charge (∼−2.0 e), whereas boron atoms are slightly positive. This fact

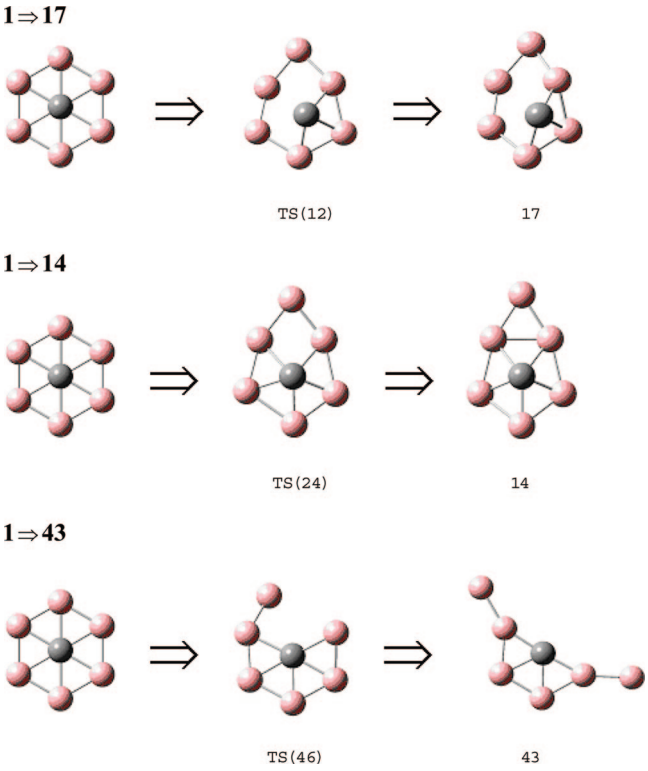

Figure 5. Three discovered dissociation channels of cyclic $(B_6C)^{-2}$ to its immediate neighborhood minima. Gray spheres are carbon atoms, whereas pink spheres are boron atoms.

TABLE 10: Computed Kinetic Barriers and Also Relative Stabilities (kcal mol^{-1}) of Relevant Intermediates for Discovered Destruction Channels of Cyclic $B_6C^{(-2)}$

	structures						
method/basis set	1	14	17	43	24[a]	12[a]	46[a]
B3LYP/6-311+g(3d2f)	0.0	32.0	31.8	28.8	40.1	42.7	49.5
B3LYP/6-311+g(3d2f)[b]	0.0	30.8	30.2	26.7	38.5	40.5	47.2
CCSD(T)/6-311+g(d)[b]	0.0	29.4	24.3	32.0	35.8	38.6	46.9
CCSD/6-311+g(df)[b]	0.0	32.3	30.2	33.8	41.4	41.8	49.0

[a] 24 = TS(1−14), 12 = TS(1−17), 46 = TS(1−43). See Figure 5 for details. [b] All B3LYP results are ZPE-corrected, whereas CCSD and CCSD(T) single point calculations were done at B3LYP/6-311+g(3d2f) optimized geometry without ZPE corrections.

may also be utilized to rationalize the exclusive stability of C_{6v} (or C_s) geometries in regard to that of C_{2v} structures. If one assumes that the electrostatic interactions are dominant factors of metal−ring interactions, then one intuitively expects that a structure to be preferred with the least distance between the most positive (metal) and negative (carbon) centers, and C_{6v} (or C_s) structure fulfills this condition. Their dominance in ab initio calculations may be interpreted in favor of an electrostatic model.

We may now proceed to scrutinize the bonding nature of metals and the cyclic dianion. Figure 3 demonstrates that at the equilibrium geometry of the C_{6v} structures metals are *bonded* only to the central carbon atom. A single bond critical point mediates this bonding. Table 6 offers the relevant topological characteristics of this critical point in all considered complexes at both the B3LYP/6-311+g(2df) and MP2/6-311+g(2df) levels. The low values of charge density, positive sign of the Laplacian of charge density ($\nabla^2\rho_c > 0$), close to zero energy density ($H_b \approx 0$), and the high ratio of kinetic energy density to the charge density ($G_c/\rho_c > 1$) are all in line with the putative "closed shell interactions".[41,81−83] This observation may be interpreted as conclusive evidence in favor of the *ionic* nature of the bonding interactions between metal and carbon atoms. This is also an independent test that vividly demonstrates the importance of electrostatic interactions in these complexes. A detailed inspection of this table reveals that once again some minor (but evident) deviations seem to exist for (M = *Be*) at B3LYP/6-311+g(2df) and also (M = *Be*) and (M = *Mg*) at the MP2/6-311+g(2df) level. These deviations and also the previously mentioned deviations from point charge electrostatic model could be explained in a unified model. This model is offered in a subsequent subsection.

3.5. Role of Charge Polarization in Be(B_6C) and Mg(B_6C) Complexes. Our computational results that were offered in previous subsections demonstrate that the closed shell electrostatic interactions have dominant contribution to the metal−ring interactions. The main obstacle with this picture was the inconsistency of the point charge model in two special cases, namely (M = *Be*) and (M = *Mg*). Since no evidence was found in favor of shared interactions, it is reasonable to concentrate on *local* modifications to this electrostatic model to account for observed anomalies. The most immediate proposal to modify this model is introducing charge distributions instead of point charges. Indeed, within the theory of intermolecular forces, sophisticated strategies such as *multipole interaction model* were developed to take account of interactions of two charge distributions or a charge distribution and a point charge.[84] The first dominant term in multipole expansions (assuming convergence of this expansion) is charge−charge interaction, whereas charge−dipole and dipole−dipole interactions must be considered in second place. Thus, if we assume that higher order terms that are involved in the electric dipole moments become important in metal−ring interactions of Be(B_6C) and Mg(B_6C) complexes, then this must be somehow extractable from QTAIM. Indeed, within this theoretical framework, total electric dipole moment of a molecule may decompose into the vector sum of interatomic and intra-atomic contributions. The polarization of charge density within an atomic basin must be evident in its intra-atomic dipole moment. Therefore, to check our hypothesis regarding the importance of polarization and multipole interactions, intra-atomic dipole moments were calculated at the B3LYP/6-311+g(2df) level. Table 7 compresses the final results for metal atoms and carbon basin. It is evident from this table that electric dipole moments are oriented on a hypothetical axis (denoted arbitrarily as *z*-axis) that is perpendicular to the ring plane and goes through the metal and carbon nuclei. The other two directions (*x*- and *y*-axes) make negligible contribution to the total intra-atomic dipole moments. This directional preference could be interpreted as the first evidence in favor of directional polarization of metal and carbon atoms. On the other hand, the magnitude of electric dipole moment of all considered metal atoms is lower than that of the carbon basin. This fact seems to be in line with both topological analysis and also the computed atomic charges. According to our previous calculations, carbon basin is the center of charge accumulation and we are faced with a flat charge distribution in this basin; both facts confirm that the carbon atom acts as a *soft* anion. This soft anion may be polarized in the presence of a positive center. Indeed, in contrast to the calculated intra-atomic dipole moment of metal atoms, the dipole moment of carbon basin varies considerably according to the considered complex. This point needs a detailed discussion.

In the alkaline series, the electric dipole moment diminishes from (M = *K*) to (M = *Li*). On the other hand, the reverse is observed for carbon basins. Intuitively, one expects that smaller

TABLE 11: Computed Kinetic Barriers and Also Relative Stabilities (kcal mol^{-1}) of Relevant Intermediates for Discovered Destruction Channels of Cyclic M[B_6C]$^{(-1)}$ Complexes (M = *Li*, *Na*, *K*)[a]

complex[b]	channels										
$Li(B_6C)^{(-1)}$											
	1	A_1	A_2	A_3	A_4	A_5	$TS(A_1)$	$TS(A_2)$	$TS(A_3)$	$TS(A_4)$	$TS(A_5)$
	0.0	30.8	35.6	67.4	52.5	47.2	51.6	48.9	67.8	54.6	51.3
	0.0	29.2	33.6	65.0	50.1	44.7	49.3	46.1	65.0	52.1	48.3
$Na(B_6C)^{(-1)}$											
	1	B_1	B_2	B_3	B_4	$TS(B_1)$	$TS(B_2)$	$TS(B_3)$	$TS(B_4)$		
	0.0	16.0	31.3	37.2	37.9	42.3	44.6	49.9	44.1		
	0.0	15.3	29.4	35.9	35.9	40.1	42.1	47.6	41.6		
$K(B_6C)^{(-1)}$											
	1	C_1	C_2	C_3	C_4	$TS(C_1)$	$TS(C_2)$	$TS(C_3)$	$TS(C_4)$		
	0.0	18.5	35.4	44.9	45.0	46.3	45.9	55.1	52.1		
	0.0	17.9	33.4	43.3	42.6	44.1	43.3	52.5	49.4		

[a] Each destruction channel is abbreviated by a symbol and a subscript. The graphical representation of transition states and intermediates may be found in Figures 6, 7, and 8. [b] The whole calculations were done at the B3LYP/6-311+g(2df) level. The first row for each complex offers the electronic energies relative to the cyclic complex (abbreviated as 1), whereas the second row contains zero point-corrected results.

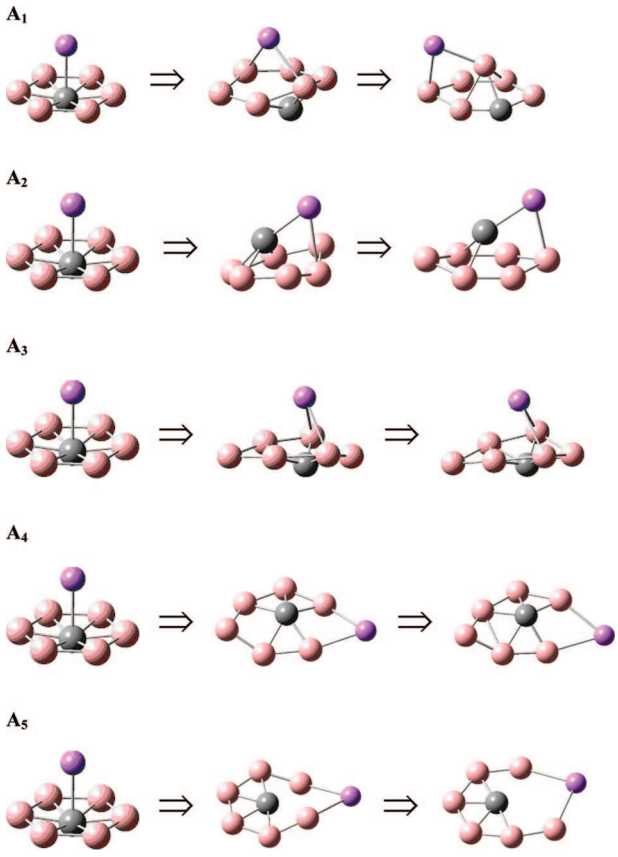

Figure 6. Five discovered dissociation channels of cyclic $Li(B_6C)^{-1}$ complex that connect it to its immediate neighborhood minima. Gray and violet spheres are carbon and metal atoms, respectively, whereas pink spheres are boron atoms. The structures in the middle of shape are transition states whereas those on the right hand are local minima.

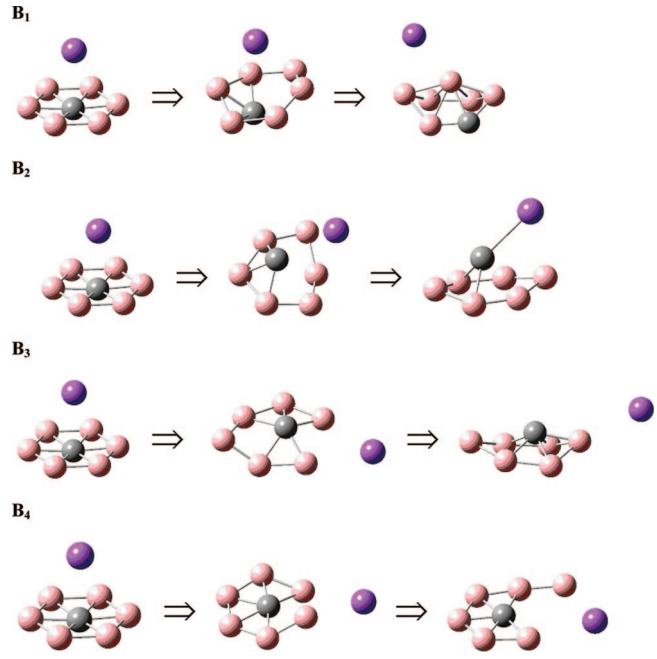

Figure 7. Four discovered dissociation channels of cyclic $Na(B_6C)^{-1}$ complex that connect it to its immediate neighborhood minima. Gray and violet spheres are carbon and metal atoms, respectively, whereas pink spheres are boron atoms. The structures in the middle of the shape are transition states, whereas those on the right hand are local minima.

cations be less polarizable (*harder*), and the counterpart anions are polarized more efficiently with harder cations. The numerical trends in Table 7 confirm our chemical intuition.

In the alkaline earth series, the electric dipole moments of metal basins are almost constant (slightly increase from (M = *Ca*) to (M = *Be*)), whereas for carbon basin it increases unusually from (M = *Ca*) to (M = *Be*). The carbon atom in $Be(B_6C)$ complex has the largest intra-atomic dipole moment. In other words, we are faced with large polarization of this basin toward beryllium (and also to some extent magnesium) basin. This large electric dipole moment clearly reveals the origin of deviation from the point charge model. The predicted dissociation energy of the $Be(B_6C)$ complex, employing QTAIM derived atomic charge of metal atom, is lower than ab initio results. Therefore, it seems reasonable to attribute the extra stability of $Be(B_6C)$ (and probably $Mg(B_6C)$ to a lesser extent) to the charge−dipole interactions that are apparently less important in other complexes. To estimate the precise energetic contribution of polarization effects, a quantitative model of these *second-order* interactions is needed. At the moment, we do not have access to such model.

It is important to stress that, although the proposed electrostatic model confirms previous identification of metal−ring interactions as ionic, it goes beyond mere description of a known fact since it predicts that *hard* cations may stabilize the polarizable ring more efficiently than *soft* cations. This important observation may be utilized (and tested) for future design of

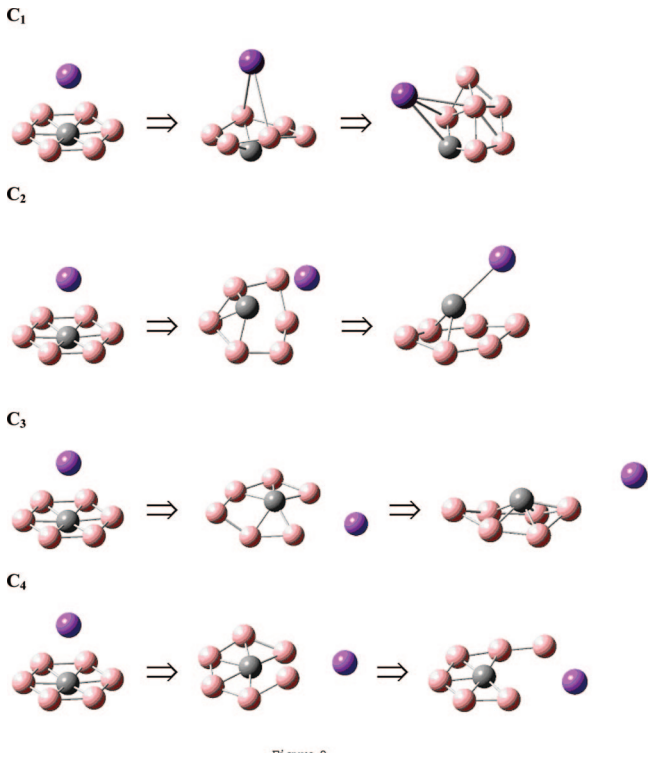

Figure 8. Four discovered dissociation channels of cyclic $K(B_6C)^{-1}$ complex that connect it to its immediate neighborhood minima. Gray and violet spheres are carbon and metal atoms, respectively, whereas pink spheres are boron atoms. The structures in the middle of the shape are transition states, whereas those on the right hand are local minima.

novel and in the same instance stable complexes with small but multiply charged cations. The transition metals could be invoked for this goal although the involvement of filled d orbitals may act as a new source of metal−ring interactions.

The near constancy of atomic charges of metal atoms in alkaline-ring series as well as varied metal charges in alkaline earth-ring series also needs explanation. Although, on the basis of our calculations, we could not propose a special mechanism for this fact, the d−π interactions (unfilled d orbitals of metal and the filled π orbitals of the ring) were invoked previously to explain the variation of atomic charges.[31,34] One intuitively expects that the importance of d−π interactions diminish from (M = *K*) to (M = *Li*) since the s−d separation gap is considerably larger in the metal atoms of the first and also second rows of periodic table. The observed trends of atomic charges demonstrate that these interactions are totally absent or at least unimportant in alkaline−ring complexes since there is no serious difference between the charge content of metal atoms. On the other hand, this problem is more intricate in alkaline earth−ring complexes. Although in line with the d−π model, the calcium atom bears less positive charge than the magnesium atom, but the atomic charge of the beryllium atom that is less than the magnesium atom does not fit into this model. It seems probable that anomalous behavior of the beryllium atom is somehow linked to the polarization effects, although this remains to be verified. Consequently, by taking all these observations into account, the d−π model seems to have limited application in these complexes.

3.6. Are Cyclic $(B_6C)^{-2}$ and Relevant Complexes Experimentally Viable Targets? Although PES of the three negatively charged species were predicted in one of the previous subsections, the main question remains unanswered: whether they are experimentally viable. This is a subtle problem because many known local minima in theoretical literature have not yet been detected with current experimental setups. This is a more serious problem when an optimized structure is not global minimum. Thus, kinetic stability is an important factor to verify the experimental viability of a local minimum, although it is usually hard to assess this factor systematically. Comparison with similar species may shed some light on this problem. Indeed, recently in joint experimental and theoretical studies, the team led by Wang and Boldyrev reported the production and spectroscopic characterization of the cyclic $(B_7C)^{-1}$ as well as $(B_6C)^{-1}$ and $(C_2B_5)^{-1}$ species.[85,86] Their detailed considerations demonstrate unambiguously that the observed structures are *not* boron wheels with a hypercoordinate carbon atom in the center of the ring. In the experimentally observed structures, carbon atoms were located in the rim of these structures. The ab initio calculations also confirm that the observed structures are ∼63 kcal mol^{-1} (in the case of $(B_7C)^{-1}$) and ∼34 kcal mol^{-1} (in the case of $(B_6C)^{-1}$) more stable than the boron wheels with a central hypercoordinate carbon atom. Therefore, these results cast some doubt on the viability of boron rings containing a central hypercoordinate carbon atom. To verify the gas-phase stability of the cyclic structure, we did a comprehensive search on its potential energy hypersurface. First, we will consider the naked dianion.

More than 500 initial structures were constructed for geometry optimization. From this set, 101 structures (63 local minima and 38 transition states) emerged (see Supporting Information for a comprehensive data set). To facilitate communication and also to prevent any ambiguity, an integer is associated with each structure and this number (this is bold and italic throughout this text) will be used to recall the relevant structure. These integers may be found in the first column of Table 8 as well as in Supporting Information. The main observed trends are as follows.

The cyclic $B_6C^{(-2)}$, ***1***, is *not* the global minimum of its potential energy hypersurface. This could be verified easily from Table 8. Accordingly, from the set of 63 optimized local minima, 12 structures are more stable than this cyclic dianion. These are depicted in Figure 4. The most stable structures (hopefully the global minima) are probably the structures ***9*** or ***20*** that are ∼39 kcal mol^{-1} more stable than cyclic dianion. These trends are also in line with a recent study.[86] Although this energy gap is less than the similar gap (which is ∼63 kcal mol^{-1}) of the cyclic and global minimum on the potential energy hypersurface of $B_7C^{(-1)}$, there is no doubt that such an energy gap suffices to claim that, in thermal equilibrium, no traces of cyclic structure could be detected.[86] Because the general numerical trends are independent of the employed computational levels (compare Tables 8 and S3 and S4 in the Supporting Information), it is safe to claim that the kinetic stability of ***1*** could be only invoked to possibly detect this structure.

To verify the kinetic stability of the cyclic structure, an extensive search was done to locate the paths (mechanisms) of transformation of this structure to each of these 12 more stable isomers. Tables 9 and S5 in the Supporting Information offer the final results, whereas Figure S1 in the Supporting Information depicts all relevant intermediates and transition states. In this regard, at least a single destruction channel was found to transform the cyclic dianion to each of these more stable isomers. All our attempts to locate *direct* transition states between the cyclic structure and these isomers failed. Hence, various intermediates were invoked to connect the cyclic structure to these isomers. It is interesting that, in all considered

destruction channels, the immediate local minima relative to the cyclic structure were found to be less stable (more than 20 kcal mol^{-1}). This clearly demonstrates that the structure ***1*** is a deep minimum relative to its immediate neighborhood minima. One may speculate that the proposed aromaticity of cyclic dianion may have some role in its relative stability.[19,33]

In all considered destruction channels, the first step of destruction is a simple transformation of structure ***1*** to one of the three ***14***, ***17***, ***43*** structures. Figure 5 depicts these primary one-step transformations. Since these are the only local minima that are directly connected to the cyclic dianion, therefore, the barrier heights of these one-step transformations are crucial for a reliable estimate of the kinetic stability of the cyclic structure. Table 10 offers final numerical estimations based on our best computational levels. At none of the employed computational levels, irrespective of the method and basis set, are the barrier heights of these transformations less than 35 kcal mol^{-1}. The general agreement of all the employed computational levels, namely, B3LYP/6-311+g(2df), B3LYP/6-311+(3d2f), CCSD/6-311+(df), CCSD(T)/6-311+g(d), and CCSD(T)/aug-cc-pVDZ, makes us confident that this estimation must be reliable. On the other hand, these results also confirm the reliability of our original estimates based on the B3LYP/6-311+g(2df) level. The extra stability of the cyclic dianion relative to its immediate neighborhood minima as well as the relatively large barrier heights for its transformation to these minima clearly demonstrate that this cyclic dianion indeed resists toward deformation and consequently destruction.

As a final step, the role of countercations was considered in the kinetic barriers. In this regard, the (M = *Li*, *Na*, *K*) series was employed. Table 11 contains the final results at the B3LYP/6-311+g(2df) level, whereas Figures 6−8 depict the structural details of these one-step transformations. It is evident that incorporation of metal cations generally elevates the barrier heights of all destruction channels. This is more pronounced for (M = *Li*) where none of the barriers are less than 46 kcal mol^{-1}. Therefore, the considered metal complexes of cyclic dianion are even more resistant toward deformation and destruction than the naked dianion. Although these results seem to be promising because the details of cluster formation in gas phase are not known, it is hard to assess theoretically the possibility of forming proper complexes. It could only be insisted that, if somehow prepared in proper conditions, at least some metal complexes of cyclic dianion must be stable enough to be detectable in gas phase or in molecular beams.

4. Summary and Prospects

Various aspects of the metal$-(B_6C)^{-2}$ complexes were considered in this article. These encompass geometries, the relative stability of relevant low energy conformers, photoelectron spectra, topological analysis of charge densities, kinetic stability, and QTAIM results. Although it is hard to assess the experimental viability of these species, on the basis of presented computational results as well as the other recent computational contributions,[31,34,39,40] there is less doubt about their possible properties if traceable. The modified electrostatic model is probably the most important achievement of this contribution since it could be employed to explain the known geometric, energetic, and electronic regularities. Additionally, it could be utilized as a guide for more efficient design of novel complexes of this dianion. This is an area with many potential applications, although the role of filled d orbitals remains to be considered in more detail. The kinetic stability of compounds containing a hypercoordinate carbon is a crucial issue for successful design of viable synthetic targets. This is particularly important since the mentioned molecules are not usually global or even low-lying minima. The cyclic $B_6C^{(-2)}$ is not an exception as well. Our analysis in this article demonstrates that there are many more stable local minima on its potential energy hypersurface. Therefore, the thermodynamic instability of this cyclic structure is revealed. On the other hand, we found that this structure and its metal complexes are more stable relative to their immediate neighborhood minima and there are appreciable barrier heights for corresponding transformations. These data seem to favor the kinetic stability of the cyclic structure.[87,88] The bulk synthesis of these complexes is another important issue that remains to be considered in future computational studies. The sensitivity of this ring to the usual environmental reagents (atmospheric oxygen, moisture, counterions, etc.) and also potential self-aggregations must be verified to devise a reasonable synthetic strategy. Much remains to be done in this area.[89]

Acknowledgment. We are grateful to Professor S. W. Ng for making the software (G98W) and hardware (machine time) facilities available, which were required for this project. S.S. is especially grateful to Prof. A. I. Boldyrev for his assistance and helpful comments on TD-DFT calculations. He is also grateful to Farnaz Heidarzadeh, Reza Hossian-nejad, and Behrouz Pezeshkian for their assistance to enhance the quality of English in this article. The fruitful comments of two anonymous reviewers greatly helped us to enhance the technical quality of this article.

Supporting Information Available: Optimized structures and total energies and zero point corrections of all considered complexes and the isomers of cyclic $B_6C^{(-2)}$. This material is available free of charge via the Internet at http://pubs.acs.org.

References and Notes

(1) Zhai, H.-J.; Alexandrova, A. N.; Birch, K. A.; Boldyrev, A. I.; Wang, L.-S. *Angew. Chem., Int. Ed.* **2003**, *42*, 6004.
(2) Zhai, H.-J.; Kiran, B.; Li, J.; Wang, L.-S. *Nat. Mater.* **2003**, *2*, 827.
(3) Kiran, B.; Bulusu, S.; Zhai, H.-J.; Yoo, S.; Zeng, X. C.; Wang, L.-S. *Proc. Natl. Acad. Sci. U.S.A.* **2005**, *102*, 961.
(4) Alexandrova, A. N.; Boldyrev, A. I.; Zhai, H.-J.; Wang, L.-S. *Coord. Chem. Rev.* **2006**, *250*, 2811.
(5) Zubarev, D. Yu.; Boldyrev, A. I. *J. Comput. Chem.* **2007**, *28*, 251.
(6) Ritter, S. K. *Chem. Eng. News* **2004**, *82*, 28.
(7) Pei, Y.; Zeng, X. C. *J. Am. Chem. Soc.* **2008**, *130*, 2580.
(8) Liebman, J. F.; Greenberg, A. *Chem. Rev.* **1976**, *76*, 311.
(9) Komarov, I. V. *Russ. Chem. Rev.* **2001**, *70*, 991.
(10) Hoffmann, R.; Alder, R. W.; Wilcox, C. F. *J. Am. Chem. Soc.* **1970**, *92*, 4992.
(11) Keese, R. *Chem. Rev.* **2006**, *106*, 4787.
(12) Minikin, V. I.; Minyaev, R. M.; Hoffmann, R. *Russ. Chem. Rev.* **2002**, *71*, 869.
(13) Jemmis, E. D.; Jayasree, E. G.; Parameswaran, P. *Chem. Soc. Rev.* **2006**, *35*, 157.
(14) Merino, G.; Méndez-Rojas, M. A.; Vela, A.; Heine, T. *J. Comput. Chem.* **2007**, *28*, 362.
(15) Minyaev, R. M.; Minikin, V. I. *Russ. J. Gen. Chem.* **2008**, *78*, 732.
(16) Gribanova, T. N.; Minyaev, R. M.; Minikin, V. I. *Russ. J. Gen. Chem.* **2008**, *78*, 750.
(17) Röttger, D.; Erker, G. *Angew. Chem., Int. Ed.* **1997**, *36*, 812.
(18) Erker, G. *Chem. Soc. Rev.* **1999**, *28*, 307.
(19) Exner, K.; Schleyer, P. v. R. *Science* **2000**, *290*, 1937.
(20) Wang, Z.-X.; Schleyer, P. v. R. *Science* **2001**, *292*, 2465.
(21) Wang, Z.-X.; Schleyer, P. v. R. *Angew. Chem., Int. Ed.* **2002**, *41*, 4082.
(22) Erhardt, S.; Frenking, G.; Chen, Z.; Schleyer, P. v. R. *Angew. Chem., Int. Ed.* **2005**, *44*, 1078.
(23) Ito, K.; Chen, Z. F.; Corminboeuf, C.; Wannere, C. S.; Zhang, X. H.; Li, Q. S.; Schleyer, P. v. R. *J. Am. Chem. Soc.* **2007**, *129*, 1510.
(24) Minyaev, R. M.; Gribanova, T. N. *Russ. Chem. Bull.* **2000**, *49*, 783.
(25) Minkin, V. I.; Minyaev, R. M. *Mendeleev Commun.* **2004**, 43.

(26) Minyaev, R. M.; Gribanova, T. N.; Minkin, V. I. *Dokl. Chem.* **2004**, *396*, 122.
(27) Minyaev, R. M.; Minkin, V. I.; Gribanova, T. N.; Starikov, A. G. *Mendeleev Commun.* **2004**, 47.
(28) Minyaev, R. M.; Gribanova, T. N.; Starikov, A. G.; Minkin, V. I. *Dokl. Chem.* **2002**, *382*, 41.
(29) Minyaev, R. M.; Gribanova, T. N. *Russ. Chem. Bull.* **2005**, *54*, 533.
(30) Li, S.-D.; Miao, C.-Q.; Ren, G.-M.; Guo, J.-C. *Eur. J. Inorg. Chem.* **2006**, 2567.
(31) Li, S.-D.; Guo, J.-C.; Miao, C.-Q.; Ren, G.-M. *Angew. Chem., Int. Ed.* **2005**, *44*, 2158.
(32) Wu, Y.-B.; Yuan, C.-X.; Yang, P. *J. Mol. Struct.: THEOCHEM* **2006**, *765*, 35.
(33) Havenith, R. W. A.; Fowler, P. W.; Steiner, E. *Eur. J. Chem.* **2002**, *8*, 1068.
(34) Luo, Q.; Zhang, X. H.; Huang, K. L.; Liu, S. Q.; Yu, Z. H.; Li, Q. S. *J. Phys. Chem. A* **2007**, *111*, 2930.
(35) Foroutan-Nejad, C.; Shafiee, G. H.; Sadjadi, A.; Shahbazian, Sh. *Can. J. Chem.* **2006**, *84*, 771.
(36) Shahbazian, Sh. *Chem. Phys. Lett.* **2007**, *443*, 147.
(37) Shahbazian, Sh.; Sadjadi, A. *J. Mol. Struct.: THEOCHEM* **2007**, *822*, 116.
(38) Islas, R.; Heine, T.; Ito, K.; Schleyer, P. v. R.; Merino, G. *J. Am. Chem. Soc.* **2007**, *129*, 14767.
(39) Li, S.-D.; Miao, C.-Q.; Guo, J.-C. *J. Phys. Chem. A* **2007**, *111*, 12069.
(40) Yang, L.-M.; He, H.-P.; Ding, Y.-H.; Sun, C.-C. *Organometallics* **2008**, *27*, 1727.
(41) Bader, R. F. W. *Atoms in Molecules: A Quantum Theory*; Oxford University Press: Oxford, 1990.
(42) Boldyrev, A. I.; Wang, L.-S. *Chem. Rev.* **2005**, *105*, 3716.
(43) Wang, L. S.; Cheng, H.-S.; Fan, J. *J. Chem. Phys.* **1995**, *102*, 9480.
(44) Wang, L.-S.; Wu, H. In *Advances in Metal and Semiconductor Clusters*; Duncan, M. A., Ed.; JAI Press: Greenwich, CT, 1998; Vol. 4, p 299.
(45) Wang, L.-S.; Li, X. In *Clusters and Nanostructure Interfaces*; Jena, P., Khanna, S. N., Rao, B. K., Eds.; World Scientific: River Edge, NJ, 2000; p 293.
(46) Møller, C.; Plesset, M. S. *Phys. Rev.* **1934**, *46*, 618.
(47) Pople, J. A.; Krishnan, R.; Schlegel, H. B.; Binkley, J. S. *Int. J. Quantum Chem. Symp.* **1979**, *13*, 325.
(48) Becke, A. D. *J. Chem. Phys.* **1993**, *98*, 5648.
(49) Becke, A. D. *Phys. Rev. A* **1988**, *38*, 3098.
(50) Lee, C.; Yang, W.; Parr, R. G. *Phys. Rev. B* **1988**, *37*, 785.
(51) McLean, A. D.; Chandler, G. S. *J. Chem. Phys.* **1980**, *72*, 5639.
(52) Krishnan, R.; Binkley, J. S.; Seeger, R.; Pople, J. A. *J. Chem. Phys.* **1980**, *72*, 650.
(53) Clark, T.; Chandrasekhar, J.; Spitznagel, G. W.; Schleyer, P. v. R. *J. Comput. Chem.* **1983**, *4*, 294.
(54) Frisch, M. J.; Pople, J. A.; Binkley, J. S. *J. Chem. Phys.* **1984**, *80*, 3265.
(55) Ortiz, J. V. *J. Chem. Phys.* **1988**, *89*, 6348.
(56) Zakrzewski, V. G.; Ortiz, J. V. *Int. J. Quantum Chem.* **1995**, *53*, 583.
(57) Ortiz, J. V.; Zakrzewski, V. G.; Dolgounircheva, O. In *Conceptual Perspectives in Quantum Chemistry*; Calais, J.-L., Kryachko, E., Eds.; Kluwer Academic: Dordrecht, The Netherlands, 1997; pp 465−518.
(58) Stratmann, R. E.; Scuseria, G. E.; Frisch, M. J. *J. Chem. Phys.* **1998**, *109*, 8218.
(59) Bauernschmitt, R.; Ahlrichs, R. *Chem. Phys. Lett.* **1996**, *256*, 454.
(60) Casida, M. E.; Jamorski, C.; Casida, K. C.; Salahub, D. R. *J. Chem. Phys.* **1998**, *108*, 4439.
(61) Frisch, M. J.; Trucks, G. W.; Schlegel, H. B.; Scuseria, G. E.; Robb, M. A.; Cheeseman, J. R.; Zakrzewski, V. G.; Montgomery, J. A., Jr.; Stratmann, R. E.; Burant, J. C.; Dapprich, S.; Millam, J. M.; Daniels, A. D.; Kudin, K. N.; Strain, M. C.; Farkas, O.; Tomasi, J.; Barone, V.; Cossi, M.; Cammi, R.; Mennucci, B.; Pomelli, C.; Adamo, C.; Clifford, S.; Ochterski, J.; Petersson, G. A.; Ayala, P. Y.; Cui, Q.; Morokuma, K.; Malick, D. K.; Rabuck, A. D.; Raghavachari, K.; Foresman, J. B.; Cioslowski, J.; Ortiz, J. V.; Baboul, A. G.; Stefanov, B. B.; Liu, G.; Liashenko, A.; Piskorz, P.; Komaromi, I.; Gomperts, R.; Martin, R. L.; Fox, D. J.; Keith, T.; Al-Laham, M. A.; Peng, C. Y.; Nanayakkara, A.; Challacombe, M.; Gill, P. M. W.; Johnson, B.; Chen, W.; Wong, M. W.; Andres, J. L.; Gonzalez, C.; Head-Gordon, M.; Replogle, E. S.; Pople, J. A. Gaussian 98, revision A.9; Gaussian, Inc.: Pittsburgh, PA, 1998.
(62) Biegler-König, F. *J. Comput. Chem.* **2000**, *21*, 1040.
(63) Biegler-König, F.; Schönbohm, J.; Bayles, D. *J. Comput. Chem.* **2001**, *22*, 545.
(64) Biegler-König, F.; Schönbohm, J. *J. Comput. Chem.* **2002**, *23*, 1489.
(65) Gonzalez, C.; Schlegel, H. B. *J. Chem. Phys.* **1989**, *90*, 2154.
(66) Gonzalez, C.; Schlegel, H. B. *J. Phys. Chem.* **1990**, *94*, 5523.
(67) Pople, J. A.; Seeger, R.; Krishnan, R. *Int. J. Quantum Chem. Symp.* **1977**, *11*, 149.
(68) Pople, J. A.; Binkley, J. S.; Seeger, R. *Int. J. Quantum Chem. Symp.* **1976**, *10*, 1.
(69) Pople, J. A.; Krishnan, R.; Schlegel, H. B.; Binkley, J. S. *Int. J. Quantum Chem.* **1978**, *14*, 545.
(70) Bartlett, R. J.; Purvis, G. D. *Int. J. Quantum Chem.* **1978**, *14*, 561.
(71) Krishnan, R.; Pople, J. A. *Int. J. Quantum Chem.* **1978**, *14*, 91.
(72) Dunning, T. H., Jr *J. Chem. Phys.* **1989**, *90*, 1007.
(73) Kendall, R. A.; Dunning, T. H., Jr.; Harrison, R. J. *J. Chem. Phys.* **1992**, *96*, 6796.
(74) Wilson, A. K.; van Mourik, T.; Dunning, T. H., Jr *J. Mol. Struct: THEOCHEM* **1997**, *388*, 339.
(75) Although because of the semi-empirical nature of the B3LYP method we tend to believe that MP2-based results are more reliable, this argument does not seem to be completely satisfactory. Since MP2-based results are also dependent on the applied basis set, the problem of stability could not be solved unequivocally by simply employing a higher level ab initio method in conjunction with a moderate size Pople-type basis set. One needs to employ extended Pople-type basis sets or switch to correlation-consistent hierarchy.[72−74] A primary calculation at the CCSD/cc-pVDZ level conforms to B3LYP results, although the energy gap is only 2.7 kcal mol^{-1}. After all, this calculation is not also conclusive.
(76) Morokuma, K. *J. Chem. Phys.* **1971**, *55*, 1236.
(77) Ziegler, T.; Rauk, A. *Inorg. Chem.* **1979**, *18*, 1558.
(78) Ziegler, T.; Rauk, A. *Inorg. Chem.* **1979**, *18*, 1755.
(79) te Velde, G.; Bickelhaupt, F. M.; Baerends, E. J.; Fonseca Guerra, C.; van Gisbergen, S. J. A.; Snijders, J. G.; Ziegler, T. *J. Comput. Chem.* **2001**, *22*, 931.
(80) Kovács, A.; Esterhuysen, C.; Frenking, G. *Chem.−Eur. J.* **2005**, *11*, 1813.
(81) Cortés-Guzmán, F.; Bader, R. F. W. *Coord. Chem. Rev.* **2005**, *249*, 633.
(82) Bader, R. F. W. *Coord. Chem. Rev.* **2005**, *249*, 3198.
(83) Macchi, P.; Sironi, A. *Coord. Chem. Rev.* **2003**, *238−239*, 383.
(84) Stone, A. J. *The Theory of Intermolecular Forces*; Clarendon Press: Oxford, 1996.
(85) Wang, L.-M.; Huang, W.; Averkiev, B. B.; Boldyrev, A. I.; Wang, L.-S. *Angew. Chem., Int. Ed.* **2007**, *46*, 4550.
(86) Averkiev, B. B.; Zubarev, D. Y.; Wang, L.-M.; Huang, W.; Wang, L.-S.; Boldyrev, A. I. *J. Am. Chem. Soc.* **2008**, *130*, 9248.
(87) Kemsley, J. *Chem. Eng. News* **2007**, *85*, 17.
(88) Roald Hoffmann was quoted in ref 87: "For a molecule to persist, at least for a few hours, these barriers (kinetic barriers) must be at least 15−20 kcal mol^{-1}" (The parentheses are from the present authors). It seems that our results fit this requirement.
(89) Our primary calculations reveal that boron atoms of this ring may react readily with boron atoms of another similar ring. No energy barrier is observed for this process, and the resultant fusion products are thermodynamically more stable than separate rings. In a recent excellent contribution, Ding and co-workers also reached similar conclusions.[40] This and similar results, which will be discussed thoroughly in a separate contribution, clearly demonstrate that, in contrast to some optimistic viewpoints, a successful design of stable metal−$(B_6C)^{-2}$ complexes in *bulk* is not a trivial task. Protection mechanisms such as those employed for bulk synthesis of aluminum or gallium clusters are probably required.[90,91]
(90) Dohmeier, C.; Robl, C.; Tacke, M.; Schnöckel, H. *Angew. Chem., Int. Ed.* **1991**, *30*, 564.
(91) Schnepf, A.; Schnöckel, H. *Angew. Chem., Int. Ed.* **2002**, *41*, 3532.

JP806874U